Chapter 4

HIGHER-ORDER VORTICES IN NONLINEAR DYNAMICAL LATTICES

***P.G. Kevrekidis**[1]*, ***B.A. Malomed**[2]*,
***D.J. Frantzeskakis**[3] **and R. Carretero-González**[4]*
[1] Department of Mathematics and Statistics,
University of Massachusetts, Amherst MA 01003-4515, USA
[2] Department of Interdisciplinary Studies, Faculty of Engineering,
Tel Aviv University, Tel Aviv 69978, Israel
[3] Department of Physics, University of Athens,
Panepistimiopolis, Zografos, Athens 15784, Greece
[4] Nonlinear Dynamical Systems Group,* Department of Mathematics and Statistics,
San Diego State University, San Diego CA, 92182, USA

Abstract

In this paper, we investigate localized discrete states with a non-zero topological charge (*discrete vortices*) in a prototypical model of dynamical lattice systems, based on the two- and three-dimensional (2D and 3D) discrete nonlinear Schrödinger (DNLS) equation, with both attractive and repulsive on-site cubic nonlinearity. Systems of two nonlinearly coupled DNLS equations are considered too. We report new results concerning the existence and, especially, stability of the vortices with higher values of the topological charge S ($S = 2, 3, 4$). Quasi-vortices, i.e., stable solutions of the quadrupole and octupole type, which replace unstable vortices with $S = 2$ and 4, respectively, are also found. The vortices of the gap-soliton type, which are found in the defocusing (repulsive) model, are quite different, as concerns the stability, from their counterparts in the focusing (attractive) models. In the two-component system, stable compound vortices of the type $(S_1, S_2) = (1, \pm 1)$ are found, the stability area being *larger* for the $(+S, -S)$ species. In the 3D case, besides finding stable vortices with $S = 1$ and 3, a novel possibility is reported, viz., a stable two-component complex with mutually orthogonal vortices in the components. Applications of the results to nonlinear optics and Bose-Einstein condensates are briefly discussed.

---

*URL: `http://nlds.sdsu.edu`

1   Introduction

In the last two decades, intrinsic localized modes in nonlinear dynamical lattices (alias *discrete breathers*) have become a topic of intense theoretical and experimental investigation, due to their inherent ability to concentrate and (potentially) transport energy in a coherent fashion; for recent reviews of the topic, see Refs. [1]. Settings in which these nonlinear excitations, strongly localized on the lattice, play an important role range from arrays of nonlinear-optical waveguides [2] to Bose-Einstein condensates (BECs) in periodic potentials [3], and from various models based on nonlinear springs [4] to Josephson-junctions ladders [5] and dynamical models of the DNA double strand [6].

One of the most ubiquitous (and, simultaneously, most convenient to examine) models in which such modes have been extensively studied is the discrete nonlinear Schrödinger (DNLS) equation [7]. Its most straightforward physical realization was found in one-dimensional (1D) arrays of coupled optical waveguides [8, 9]. Such arrays may be multi-core structures made in a slab of a semiconductor material (AlGaAs) [9] or silica [10], or virtual ones, induced by a set of laser beams illuminating a photorefractive crystal [11]. In this experimental implementation of the DNLS system, the number of lattice sites (guiding cores) is $\simeq 40$, and the available propagation distance is up to 20 diffraction lengths of the localized mode, which lends enough room to create discrete solitons and conduct various experiments with them, including collisions [12]. Very recently, discrete diffraction of light was demonstrated experimentally in a bundle of optical waveguides with a regular 2D square-lattice transverse structure, of size up to 7×7, made in fused silica [13]. Actually, lattices of a much larger size, such as 112×112, can be readily created in a photorefractive crystal, with lattice spacing $\simeq 20\mu$m.

An array of BEC droplets trapped in a strong optical lattice (OL), with $\simeq 10^3$ atoms in each droplet, is another direct physical realization of the DNLS model [3]. In this case, the DNLS equation can be systematically derived via a Wannier-function decomposition [14].

While the BEC-droplet arrangements can be one-, two- and three-dimensional (3D) [15], the optical-waveguide implementations can be, at most, two-dimensional. Another feasible physical realization of the DNLS model in the 3D case may be provided by a lattice built of tunnel-coupled microresonators trapping photons [16] or polaritons [17].

Recently, an idea of light-induced photonic lattices has emerged in nonlinear optics [18, 19, 20] (it is closely related to the above-mentioned virtual lattices used in the experiments with photorefractive media [11]). It arises from the possibility to modify the refractive index of a nonlinear medium by means of a periodic pattern of intensity modulation, created by a grid of strong beams, while a weaker beam (which, however, experiences much stronger nonlinearity) is launched in the perpendicular direction to probe the resulting structure. Promising experimental studies of discrete solitons in 2D and quasi-2D lattices were stimulated by this novel context [18, 19, 21, 22].

Theoretical studies have predicted various types of stable discrete solitons that may occur in 1D dynamical lattices, such as twisted solitons and multi-humped bound states [23], compactons [24], and several types of gap solitons [25, 26]. The recent advancements in the above-mentioned experiments strongly suggest to extend the analysis of DNLS solitons to the 2D and 3D cases. Strictly speaking, 2D photonic lattices in photorefractive materials feel a different (saturable) nonlinearity; however, they support essentially the same

robust structures as the DNLS model. On the other hand, the bundled 2D waveguide arrays, reported in Ref. [13], as well as BECs loaded into a strong 2D/3D optical lattice, are described precisely by the respective (2D/3D) DNLS model. In particular, of special interest are discrete 2D and 3D solitons carrying a topological charge, i.e., *discrete vortices*. In the context of the DNLS equation, the fundamental vortices, with the topological charge ("spin") $S = 1$, were systematically investigated in Ref. [27], as 2D counterparts of the 1D discrete twisted solitons of [23], the most important issue being their stability. Bound states of 2D DNLS solitons, including both vortex and zero-vorticity ones, were investigated in Ref. [28]. In the context of other 2D lattice models, some vorticity-carrying configurations were earlier considered in Ref. [29]. Very recently, quasi-discrete vortices were observed, and their robustness was demonstrated, in two independent experiments performed in a photonic lattice created in a photorefractive material [30, 31].

Similar vortex states, as well as higher-order vortices, and "supervortices", i.e., ring-shaped arrays built of individual vortices with global vorticity imprinted upon them, were found in a *continuum* model based on the 2D Gross-Pitaevskii (GP) equation including a square-lattice periodic potential, which describes a BEC with attractive inter-particle interactions (negative scattering length), loaded into the corresponding square OL [32]. Analogous vortex solutions were obtained in the context of a 2D phenomenological model of photonic crystals [33]. Stable vortex solitons can be found too in the 2D GP equation with hexagonal, triangular, or quasi-periodic (rather than square) OLs, and even in the case when the intrinsic interaction is repulsive [34] (in the latter case, the localized structure is of the gap-soliton type, see also Refs. [35] and [36]). Asymmetric (with respect to the geometry of the lattice) vortices were also recently examined [37].

While it was quite easy to demonstrate that the fundamental ($S = 1$) vortex solitons are stable in all the above-mentioned settings, a challenging issue concerns the stability of *higher-order* discrete vortices, with $S \geq 2$. In the case of the DNLS, a family of $S = 2$ vortices was constructed in Ref. [27]; however they were found to be unstable.

On the other hand, similar issues were recently investigated in *uniform* (i.e., without external potential) continuum models with the cubic-quintic and $\chi^{(2)} : \chi^{(3)}_{-}$ (quadratic – self-defocusing-cubic) nonlinearities. Originally, it was found that only vortex solitons with $S = 1$ and $S = 2$ were stable in the cubic-quintic model, while the ones with $S \geq 3$ were supposed to be unstable [38]. However, it was then demonstrated that the higher-order vortices may be stable too (at least, up to $S = 5$), but in very narrow regions [39]. For instance, for $S = 3$ solitons the stability domain occupies $\simeq 3\%$ of the existence region (and still less for $S > 3$), while for the fundamental ($S = 1$) vortices the relative size of the stability area was $\simeq 10\%$. More recently, similar results were obtained for the vortex solitons in the spatially uniform $\chi^{(2)} : \chi^{(3)}_{-}$ model [40], which suggests that narrow stability domains of higher-order vortex solitons is a generic feature of continuum spatially uniform models with competing nonlinear interactions.

It is relevant to mention that the stable higher-order vortex soliton beams in bulk media may be promising, in applications to photonics, as "light conduits" to guide weak optical signals, since they are "more hollow" than the beams with $S = 1$. On the other hand, if, for instance, the vortex beam with $S = 2$ is unstable against splitting into two fundamental vortices with $S = 1$, which is typical in media with a simple nonlinearity (for instance, only quadratic) [38], this may be used to create a Y-shaped ramification of the conduit.

In this work, we address the stability of higher-order vortex solitons in the 2D and 3D DNLS model. In particular, this is motivated, by the above-mentioned recent experimental demonstration of stable fundamental quasi-discrete vortex solitons [30], and availability of phase masks which can lend vorticity $S \geq 2$ to a laser beam, which is to be used for the creation of the soliton. Experimental search for such high-order spatial vortex solitons in a photorefractive lattice was recently undertaken (see e.g. Ref. [41] where an input of a charge 4 vortex gave rise to soliton necklaces). Here, we demonstrate, by means of accurate numerical calculation of eigenvalues of the linearization around such solitons, that they are *stable* in properly chosen parameter regions of the DNLS model. Also, the recent 3D experiments in BECs with OLs [15] indicate that similar structures may be present in the latter context.

The paper is organized as follows. The 2D model is formulated and examined in Section II, which also briefly describes numerical techniques employed for the analysis of solutions and their stability. Detailed results for the vortices with $S = 3$ are given. The analysis is based on the computation of the full set of the corresponding linear-stability eigenvalues. The evolution of unstable solitons is investigated by dint of direct simulations (it is found that they split into a set of two stable solitons, with $S = 1$ and $S = 0$). We also consider real solutions of the quadrupole type, which replace the vortices with $S = 2$ (recall the true complex $S = 2$ solitons are all unstable [27]); their octupole-type counterparts are briefly considered too. The vorticity of the real quadrupole (and octupole too) solitons can be directly identified only if a small perturbation, which makes them complex, is added. To this end, we employ all the localized eigenmodes of small perturbations around the solutions, and conclude that their vorticity, defined this way, is not 2, but zero. Nevertheless, it is a novel type of the localized solutions, qualitatively different from the ordinary $S = 0$ solitons, therefore we call them *quasi-vortices*. The stability region is found for the quasi-vortices adjoint to both the $S = 2$ and $S = 4$ configurations. We also examine vortices in the cases of a *defocusing* cubic nonlinearity (which corresponds to the repulsive interaction between atoms in the BEC), and identify differences of their stability characteristics from those in the focusing case. Additionally, in Section II we examine *coupled vortices* in two-component models, and report a surprising finding: a pair of coupled vortices with opposite values of the topological charge, $S_1 = -S_2$, are *more robust* (have a larger stability area) than their counterparts with $S_1 = +S_2$.

In Section III, we examine discrete vortices in the 3D DNLS model. In this case, we find stable $S = 1$ and $S = 3$ vortices. For $S = 2$ we demonstrate an unexpected feature, that unstable $S = 2$ vortices may relax *upscale*, to their stable counterparts with $S = 3$. We also highlight a new type of a compound vortex in the two-component model, which is a stable bound state of two vortices with mutually perpendicular axes. Finally, in Section IV we summarize the findings and present conclusions.

2 Two-Dimensional Vortices

2.1 The Model

The DNLS equation for the complex dynamical field $\phi_{m,n}$ (which is the atomic wave function in the BEC, or amplitude of the electromagnetic wave in the optical waveguiding array)

on the 2D square lattice has a well-known form [7],

$$i\frac{d}{dt}\phi_{m,n} + C\Delta_2\phi_{m,n} + |\phi_{m,n}|^2\phi_{m,n} = 0, \tag{1}$$

where C is the coupling constant, and Δ_2 stands for the discrete Laplacian, $\Delta_2\phi_{m,n} = \phi_{m+1,n} + \phi_{m,n+1} + \phi_{m,n-1} + \phi_{m-1,n} - 4\phi_{m,n}$. For stationary solutions, $\phi_{m,n} = \exp(i\Lambda t)u_{m,n}$, Eq. (1) leads to the time-independent equation:

$$\Lambda u_{m,n} = C\Delta_2 u_{m,n} + |u_{m,n}|^2 u_{m,n}. \tag{2}$$

Numerical solutions to Eq. (2) were obtained by means of the Newton method (note that we are interested, generally speaking, in complex solutions, therefore $u_{m,n}$ was decomposed into its real and imaginary parts).

Upon generating stationary localized solutions, their stability was examined through linearization. To this aim, a perturbed expression of the form [42],

$$\phi_{m,n} = \exp(i\Lambda t)u_{m,n}$$
$$+\epsilon\exp(i\Lambda t)[a_{m,n}\exp(-i\omega t) + b_{m,n}\exp(i\omega^* t)] \quad, \tag{3}$$

was substituted into Eq. (1). Here, $u_{m,n}$ is the unperturbed stationary solution, ϵ is an infinitesimal amplitude of the perturbation, ω is its eigenfrequency (which is imaginary or complex in the case of instability) and $(\cdot)^*$ denotes complex conjugation. This leads to the following linear equation for the perturbation eigenmodes,

$$\omega\begin{pmatrix} a_k \\ b_k^* \end{pmatrix} = \mathbf{J}\begin{pmatrix} a_k \\ b_k^* \end{pmatrix}, \tag{4}$$

where $\mathbf{J}$ is the Jacobian matrix,

$$\mathbf{J} = \begin{pmatrix} \partial F_k/\partial u_j & \partial F_k/\partial u_j^* \\ -\partial F_k^*/\partial u_j & -\partial F_k^*/\partial u_j^* \end{pmatrix}, \tag{5}$$

and $F_k \equiv -C(u_{k+1} + u_{k-1} + u_{k+N} + u_{k-N} - 4u_k) + \Lambda u_k - |u_k|^2 u_k$; the string index $k = m + (n-1)N$ maps the $N \times N$ lattice $\{m,n\}$ into a vector of length N^2. Numerical solutions were sought for with the Dirichlet boundary conditions at the domain boundaries, i.e., at $n = 1, n = N$ and $m = 1, m = N$.

We use the obvious scaling invariance of the equation to fix the frequency $\Lambda = 4$ in Eq. (2), and then vary the coupling constant C, to examine continuous branches of the solutions. This way, we can cover the entire manifold of the discrete-soliton solutions, if their integer vorticity S is varied too. It has been shown before [27] that, for the chosen value of $\Lambda = 4$, the $S = 0$ discrete solitons and the $S = 1$ fundamental vortices in the DNLS equation are stable in the regions

$$C \leq C_{\mathrm{cr}}^{(0)} = 4.0 \ \text{ and } \ C \leq C_{\mathrm{cr}}^{(1)} = 1.6, \tag{6}$$

respectively.

To generate vortex solutions with given integer S, we initialize the Newton method with a complex *ansatz* suggested by a general expression for the vortex relevant to the continuum model,

$$
\begin{aligned}
u_{m,n}^{(\text{init})} &= A[(m - m_0) + i(n - n_0)]^S \\
&\times \ \text{sech}\left(\eta\sqrt{(m - m_0)^2 + (n - n_0)^2}\right),
\end{aligned} \tag{7}
$$

where (n_0, m_0) is the location of the vortex' center, and η is its intrinsic scale parameter. To generate numerically exact stationary solutions, the Newton algorithm was iterated until a convergence no worse than 1 part in 10^8 was achieved. After that, the linear stability analysis of the stationary solutions was performed. The results are typically shown for 15×15 site lattices, but it was verified that they are only weakly affected by domain size for larger domains.

2.2 Vortices with $S = 3$

Motivated by the discovery of the stable higher-order vortex solitons in the uniform continuum models [39, 40], we started by seeking for $S = 3$ solutions in the 2D DNLS equation. Basic results for these vortices are summarized in Fig. 1. The top left panel of the figure displays the norm of the solution, $P = \sum_{m,n} |u_{m,n}|^2$ (which has the meaning of the total power of the trapped light beam in the optical waveguide array, or number of atoms in the trapped BEC) as a function of C, for fixed $\Lambda = 4$. Note that, in the quasi-continuum approximation, which corresponds to $C \gg \Lambda$, the dependence $P(C)$ must be obviously linear for 2D solitons of any type; it is noteworthy that the linear dependence pertains at smaller values of the coupling constant.

The instability growth rate of the vortex soliton, i.e., the real part of the most unstable perturbation eigenvalue $\lambda \equiv i\omega$, is shown, as a function of C, in the top middle panel of Fig. 1. The top right panel illustrates the structure of the stationary solution (for $C = 0.02$) through values of the complex field $u_{m,n}$ at the main sites constituting the vortex. The solution can be identified as corresponding to $S = 3$ through the phase variation of the field, which follows the $e^{3i\theta}$ pattern, θ being the angular coordinate in the plane. The $S = 3$ vortices are stable in the region

$$
C \leq C_{\text{cr}}^{(3)} = 0.398, \tag{8}
$$

where $\text{Re}(\lambda) \equiv 0$ [cf. the stability intervals (6) for $S = 0$ and $S = 1$ solitons]. At the point $C = C_{\text{cr}}^{(3)}$, an instability sets in through a *Hamiltonian Hopf bifurcation* [43], which is a consequence of the collision of two imaginary eigenvalue pairs with opposite *Krein signatures* (as was discussed in a general form in Refs. [44, 45]). This bifurcation results in complex quartet of eigenvalues. With subsequent increase of C, we encounter additional destabilizing bifurcations at $C = 0.402$, $C = 0.508$, $C = 0.524$, $C = 0.886$ and $C = 0.952$, which increase the number of unstable modes. This eventually results in six quartets of unstable eigenvalues at $C = 1.418$, as shown in the bottom right panel of Fig. 1. Examples of the stationary vortices and spectral planes of their stability eigenvalues, $\lambda \equiv \lambda_r + \lambda_i$, are displayed in the middle row of Fig. 1 for a stable case ($C = 0.02$), and in the bottom row for $C = 1.418$.
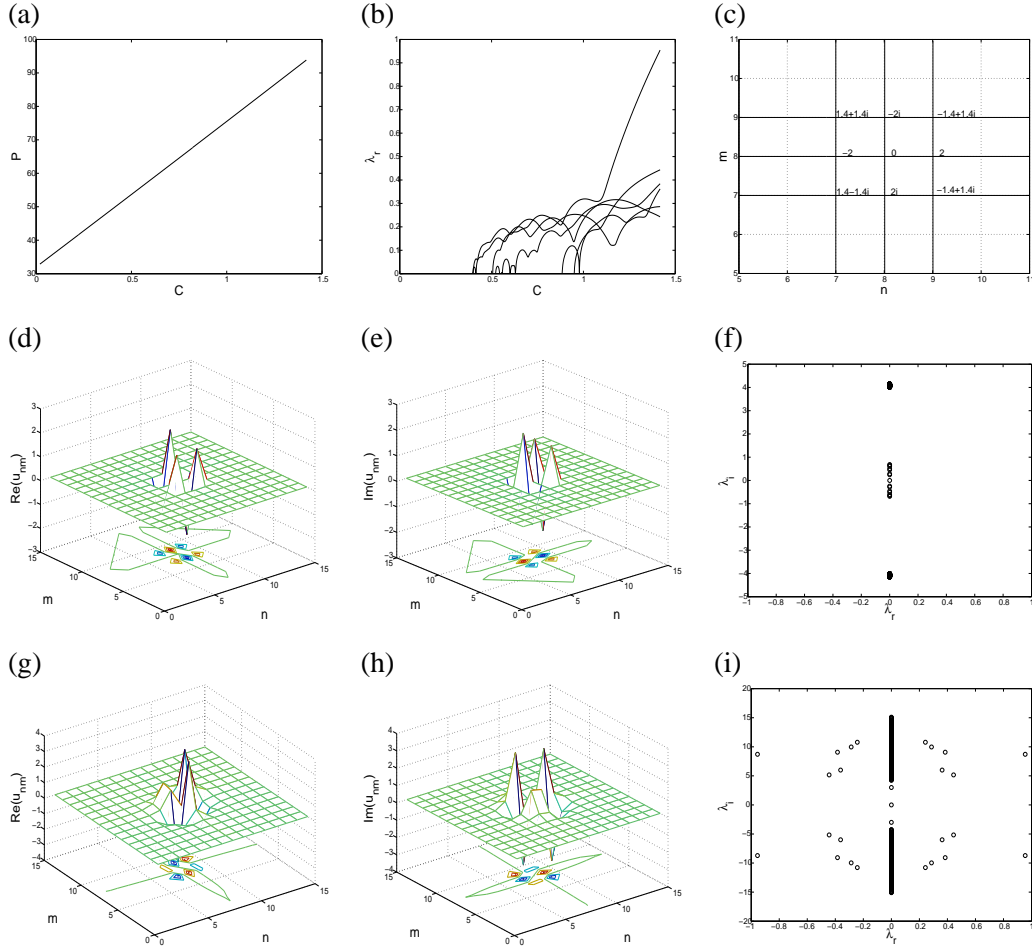
Figure 1: The top left panel shows the norm of the vortex-soliton solution with $S = 3$ vs. the lattice-coupling strength C. The real part of the most unstable eigenvalues are shown as a function of C in the top middle panel (the instability takes place at $C > 0.398$). The top right panel shows the structure of the $S = 3$ vortex through values of the complex stationary field $u_{m,n}$ at the sites where the vortex is actually located. Examples of the real and imaginary parts of the profile of the stationary solution, and of the spectral plane of its (in)stability eigenvalues are shown in the left, middle and right panels, respectively: in the middle row for $C = 0.02$ (a stable vortex), and in the bottom row for $C = 1.418$ (a strongly unstable one). Note that there may be up to six eigenvalue quartets accounting for the instability.

Nonlinear development of the instability of the $S = 3$ vortex in the region $C > C_{cr}^{(3)} = 0.398$ was examined in a number of cases by means of direct simulations of Eq. (1), using the fourth-order Runge-Kutta method; the instability was initiated by adding a small initial perturbation to the solution. A typical example is shown in Fig. 2 for the case of $C = 0.618$. In this case, the original $S = 3$ vortex splits into one with $S = 1$, which stays at the initial position, and an additional fragment with $S = 0$, which separates and eventually gets trapped at a different lattice site. Both the $S = 1$ and $S = 0$ solitons, generated by the instability from the $S = 3$ vortex, are stable at the corresponding values of the parameters. We stress that the apparent non-conservation of the topological charge observed in these simulations is quite possible, as the lattice does not conserve angular momentum.
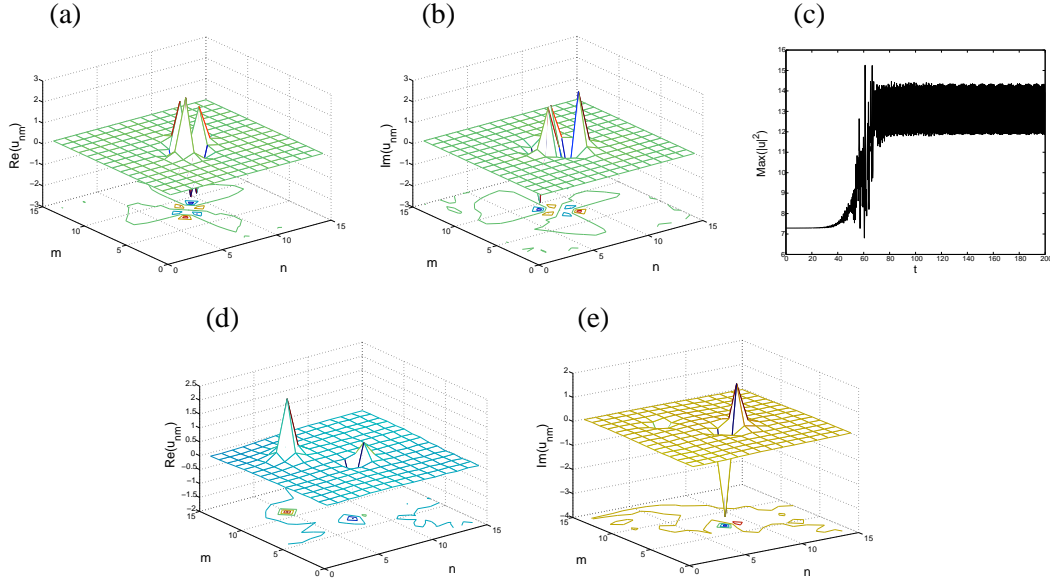

Figure 2: The two top left panels show the initial unstable $S = 3$ vortex for $C = 0.618$. The top right panel shows the beginning of the oscillatory instability in the evolution of the lattice field. The bottom panels show the real and imaginary parts of the eventually established field configuration, which contains stable solitons with $S = 0$ and $S = 1$.

2.3   Quasi-vortices ($S = 2$ and $S = 4$)

The stationary equation (2) admits real solutions, which are generated, e.g., by the real part of the ansatz (7) with $S = 2$ and $S = 4$. First, we will consider their shape and dynamical properties; then, we will discuss the interpretation of such real solutions in terms of vorticity.

For $S = 2$, typical results are shown in Figs. 3 and 4. Similar to Fig. 1, the top left and right panels in Fig. 3 show, respectively, the norm of the solution, and the instability growth rate as a function of C. As in the case of the $S = 3$ vortex, the instability sets in through

the Hamiltonian Hopf bifurcation resulting from the collision of two imaginary eigenvalue pairs with opposite Krein signatures, which gives rise to a quartet of complex eigenvalues. The stability region is

$$C \leq C_{\text{cr}}^{(2)} = 0.862 \tag{9}$$

[cf. the stability intervals (6) for $S = 0$ and $S = 1$ solitons, and (8) for $S = 3$]. The profile of the solution and the spectral plane of the stability eigenvalues associated with it are displayed for a stable case ($C = 0.02$) in the middle row, and at the instability onset, $C = 0.862$, in the bottom row of Fig. 3. It is clear that the resulting solution follows a pattern of $\cos(2\theta)$ (which relates the solution to $S = 2$), where θ is, as above, the angular variable in the plane.

Development of the instability of these solitons for $C > 0.862$ was studied by direct simulations of Eq. (1). A typical example is shown in Fig. 4 for $C = 1$: the oscillatory instability transforms the initial state into an ordinary zero-vorticity lattice soliton, which is a stable solution in this case.

The interpretation of solutions of this type in terms of the vorticity is ambiguous, as the solution is a purely real one. As is obvious from Fig. 3, the solution is actually a quadrupole localized on four lattice sites, with zero between them, which is typical for vortex solutions that must vanish at the central point. The phase of the solution jumps by π when comparing positive and negative real values of the field at adjacent sites carrying the solution. To understand the global vorticity that may be ascribed to this state, one can add a small perturbation which makes the solution complex and thus makes it possible to define a phase field across the lattice (this, obviously, corresponds to a situation expected in the experiment, where perturbations are inevitable). To this end, perturbations based on the three localized eigenmodes of small perturbations existing around the stable stationary states of the present type were tried. In Fig. 5, a full set of contour plots for the eigenmodes is displayed for the same case ($C = 0.02$) which was used as an example in Fig. 3. The most essential feature of the eigenmodes is that they are completely localized on the same set of four sites which carry the unperturbed solution.

Straightforward consideration demonstrates that a combination of the stationary solution and of the first eigenmode (the one with the eigenvalue $\lambda_1 \equiv i\omega_1 \approx 0.08i$), taken with a small amplitude, may give rise to the following phase distribution along a closed route connecting the four sites:

$$0 \rightarrow \pi \rightarrow 0 \rightarrow \pi \rightarrow 0, \tag{10}$$

or the same multiplied by (-1). In fact, the perturbed configuration oscillates, at the frequency ω_1, between these two phase patterns. Next, the second and third eigenmodes, which belong to a double eigenvalue, $\lambda_{2,3} \equiv i\omega_{2,3} \approx 0.04i$ ($\omega_{2,3}$ is not exactly exactly equal to $\omega_1/2$), if added, with a small amplitude, to the unperturbed state, may give rise to phase patterns of the types

$$0 \rightarrow \pi \rightarrow 0 \rightarrow -\pi \rightarrow 0, \text{ or } 0 \rightarrow \pi \rightarrow 2\pi \rightarrow \pi \rightarrow 0. \tag{11}$$

None of these patterns is characterized by a nonzero net phase gain generated by the round trip along the closed route, so the pattern cannot be ascribed finite vorticity. However, this is clearly a new type of stable localized 2D lattice solutions, drastically different from the ordinary zero-vorticity solitons. While this solution has no vorticity, it may be characterized
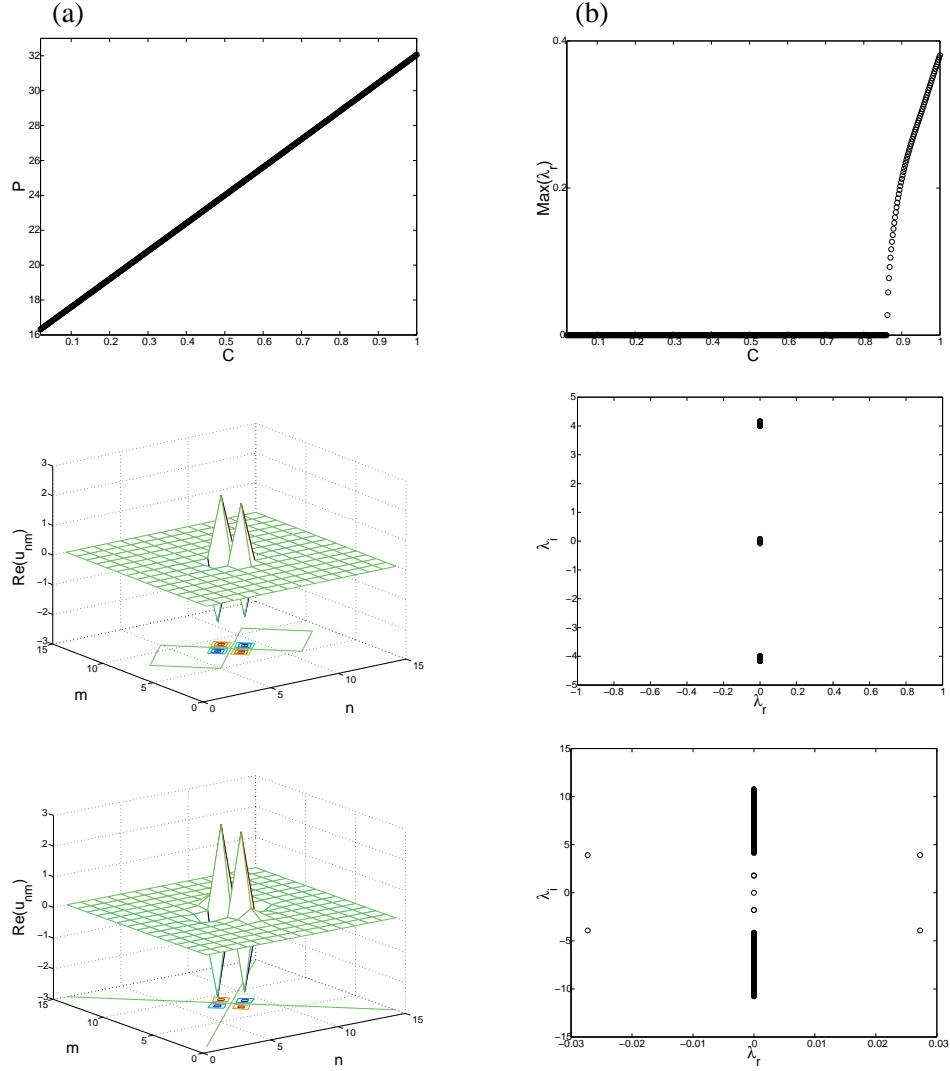
Figure 3: The top left panel shows the norm of the quasi-vortex solution, corresponding to $S = 2$, vs. the coupling constant C. The largest real part of the stability eigenvalues is shown as a function of C in the top right panel (the instability sets in at $C = 0.862$). The (purely real) profile of the stationary solution, and the spectral plane of the associated stability eigenvalues, are shown in the left and right panels: in the middle row for $C = 0.02$, and in the bottom one for $C = 0.862$.
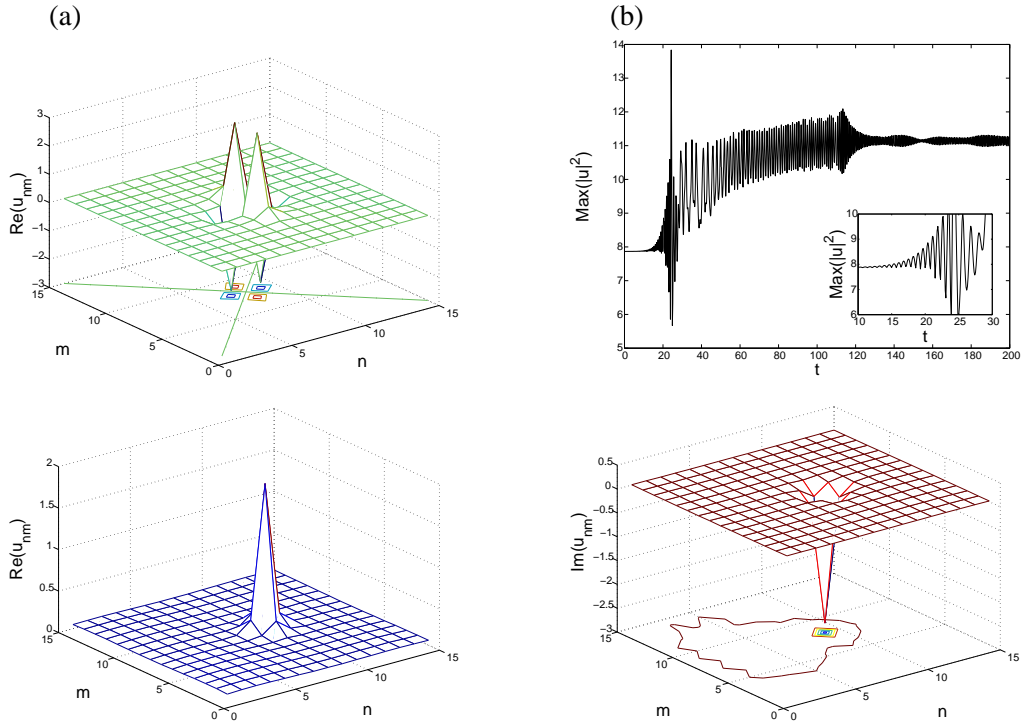
Figure 4: The top left panel shows the initial unstable quasi-vortex corresponding to $S = 2$, in the case of $C = 1$. The top right panel shows the oscillatory instability, setting in around $t = 15$, in the evolution of the lattice field. The bottom panels show the real and imaginary parts of the established stable configuration (at $t = 200$), which is identified as an ordinary stable zero-vorticity soliton.
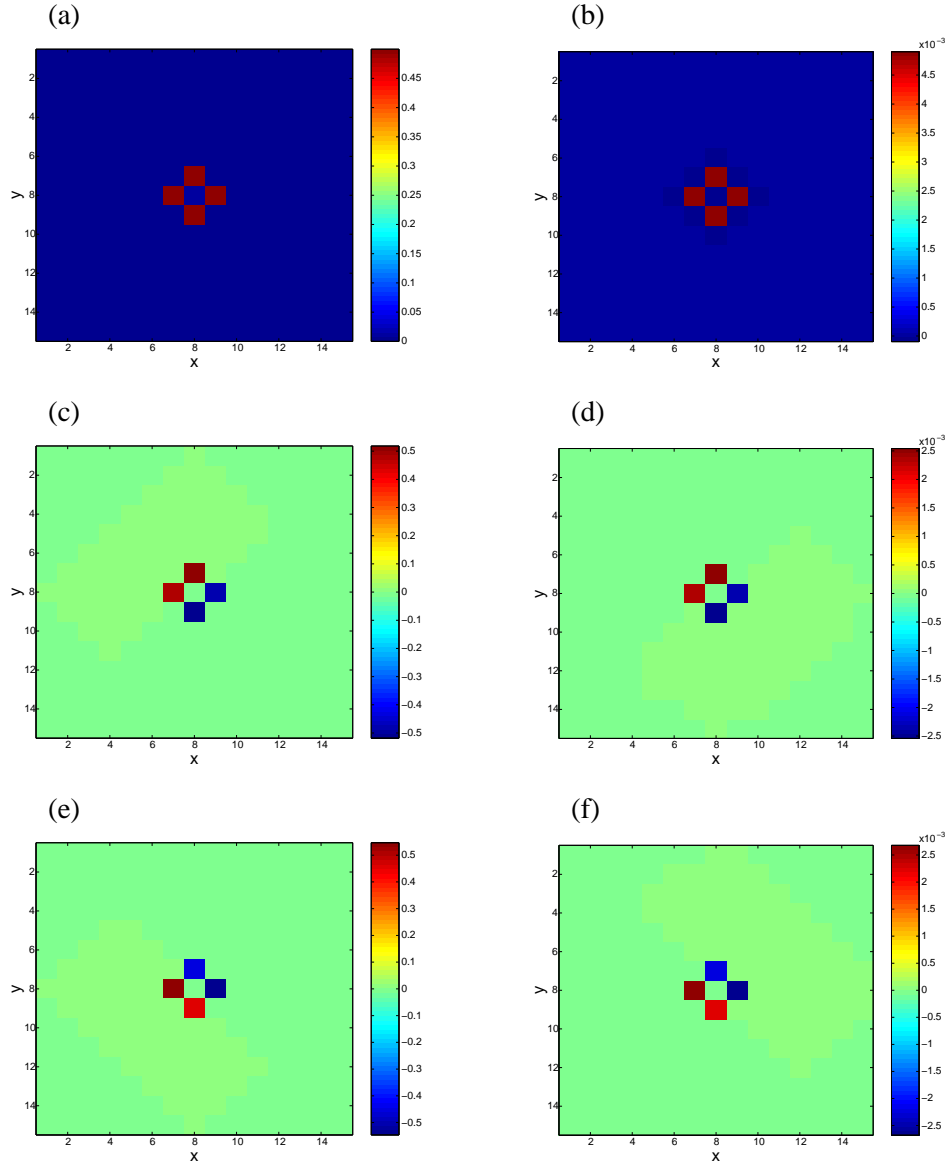
Figure 5: The panels display, in the form of contour plots, the real (left panels) and imaginary (right panels) parts of the full set of three eigenmodes of small perturbations that are localized in the case of the stable quasi-vortex for $C = 0.02$ (the same case as presented in Fig. 3). The first eigenmode (top panels) corresponds to the frequency $\omega_1 \approx 0.08$, and the two other eigenmodes (middle and bottom panels) belong to the double frequency $\omega_{2,3} \approx 0.04$.

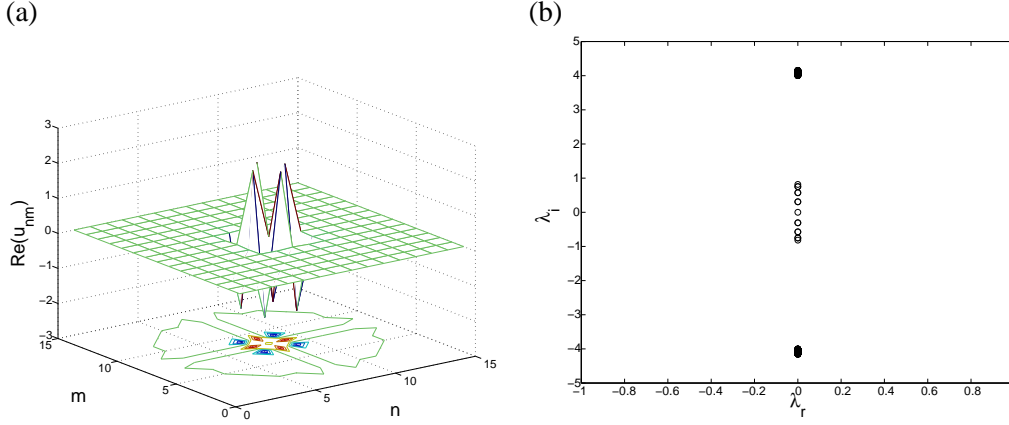(a)   (b)

Figure 6: The profile (left) and stability (right) of the quasi-vortex with $S = 4$ for $C = 0.02$. Notice that the spectral plane contains 7 pairs of eigenvalues in this case.

by the largest intrinsic phase difference, $(|\Delta\phi|)_{\max}$. This quantity depends on the way a small perturbation is added: $(|\Delta\phi|)_{\max} = \pi$ in the case of Eq. (10), and $(|\Delta\phi|)_{\max} = 2\pi$ in the case of Eq. (11). We call this type of real solutions *quasi-vortices*.

We stress that complex localized solutions to the 2D DNLS equation, that are true vortices with $S = 2$, were found in Ref. [27]. They were constructed starting with a complex ansatz, whose real and imaginary parts, unlike those in the expression (7), emulated the continuum-model's expressions of $\cos(2\theta)$ and $\sin(2\theta)$ respectively. However, it was found in Ref. [27] (and re-checked in the course of the present work) that those true vortices are *always unstable*, through a real eigenvalue pair.

We have also constructed real quasi-solitons corresponding to $S = 4$ [i.e., generated by the real part of the initial ansatz (7) with $S = 4$]. An example is given in Fig. 6 for $C = 0.02$. The stability interval of such solutions is [cf. Eqs. (8) and (9)]

$$C \leq C_{\mathrm{cr}}^{(4)} = 0.292.$$

As expected from the comparison with known results for continuum models (with competing nonlinearities) [39, 40], the stability interval shrinks (but does not disappear) with the increase of S, which equally pertains to the true vortices and quasi-vortices.

2.4   Vortices in the Repulsive Model

We have also examined Eq. (1) with the opposite sign in front of the nonlinear term, i.e., the defocusing nonlinearity. This case is relevant, e.g., to BECs with repulsive interactions in the presence of the OL, see, e.g., [3, 14, 46]. We report here, briefly, the results for vortices in this case.

It should be mentioned that the substitution $\phi_{m,n}(t) \equiv (-1)^{m+n} \exp(-8iCt) \, \tilde{\phi}_{m,n}^{*}(t)$ (the so-called staggering transformation), followed by complex conjugation, reverses the sign of the nonlinearity in the DNLS equation (1). Therefore, any ordinary (quasi-smooth)

soliton in the attractive model comes with its staggered-soliton counterpart in the repulsive model, and vice versa. To avoid dealing with essentially the same solution twice, we consider the discrete solitons in the attractive model (above and below) and in the repulsive one (in this subsection), each time starting to search for the solutions with an initial ansatz [see Eq. (7) and also Eq. (16) below] that does *not* contain the staggering factor, $(-1)^{m+n}$.
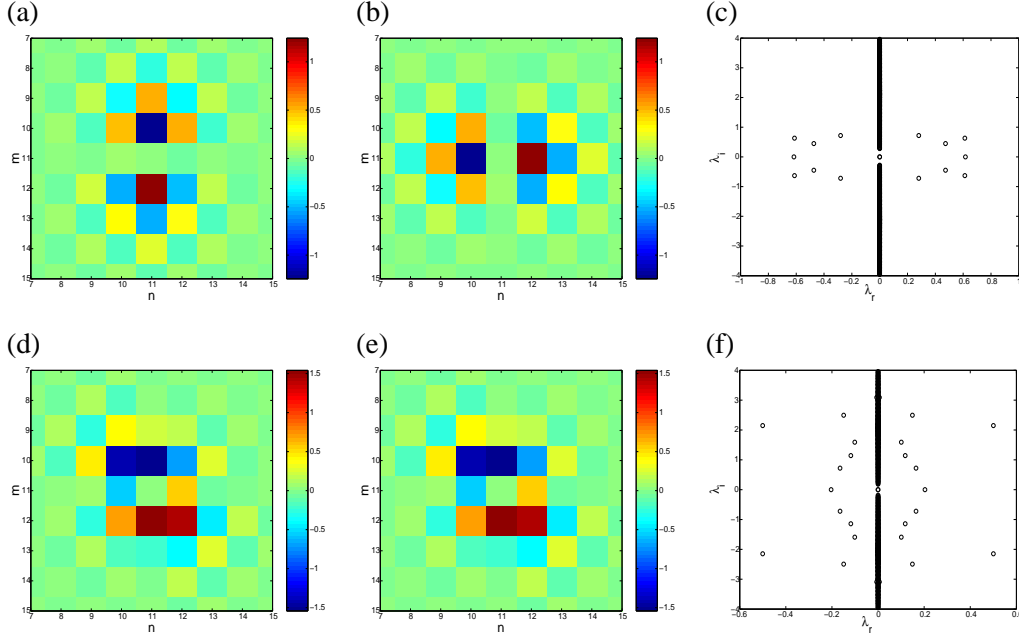

Figure 7: The top panels show the real (left) and imaginary (middle) parts of the unstable vortex with $S = 1$ in the repulsive model for $C = 0.47$ and $\Lambda = -4$ (the linear-stability spectral plane is shown in the right panel). This vortex is unstable for $C > 0.38$. The bottom panels show another branch of the solutions with $S = 1$ (in th same repulsive model), initialized with a quasi-continuum ansatz. The solution is shown for $C = 0.48$, but it is unstable at $C > 0.22$.

The stability of vortices in the repulsive model is significantly different from that of their counterparts in the attractive one. There exist multiple branches of vortices, including "more discrete" ones (which, at small values of the coupling constant, resemble the ones examined in the focusing case) and more extended states, which would be highly unstable in the attractive model (in terms of Ref. [36], these two branches are of the "tightly-bound" and "weakly-bound" types, respectively). Two such examples are shown in Fig. 7. The solutions corresponding to the strongly discrete branch gradually approach (with the increase of C) vortices of the gap-soliton type, similar to those recently found in the continuum equation with the OL in Refs. [35] and [36]. This branch becomes unstable at $C = 0.38$ (with $\Lambda = -4$), and it can no longer be traced for $C > 0.48$. The simplest branch of weakly localized vortices is also shown in the same figure. This branch becomes unstable at $C = 0.22$ and cannot be traced for $C > 0.49$ (cf. Fig. 7).

In the repulsive model, even the solitons with $S = 0$ can be of different types, i.e., strongly or weakly localized (in the continuum model with the OL, the same was found in Ref. [36]). The strongly localized solution gives rise to a discrete gap-soliton branch (which is similar to the one found in Ref. [47]) that cannot be continued for $C > 0.48$ (and appears to become unstable through a saddle-node bifurcation very close to this point), while the latter is stable for $C < 0.148$ and also disappears at large values of the coupling constant. Examples of the $S = 0$ discrete solitary waves are shown in Fig. 8.
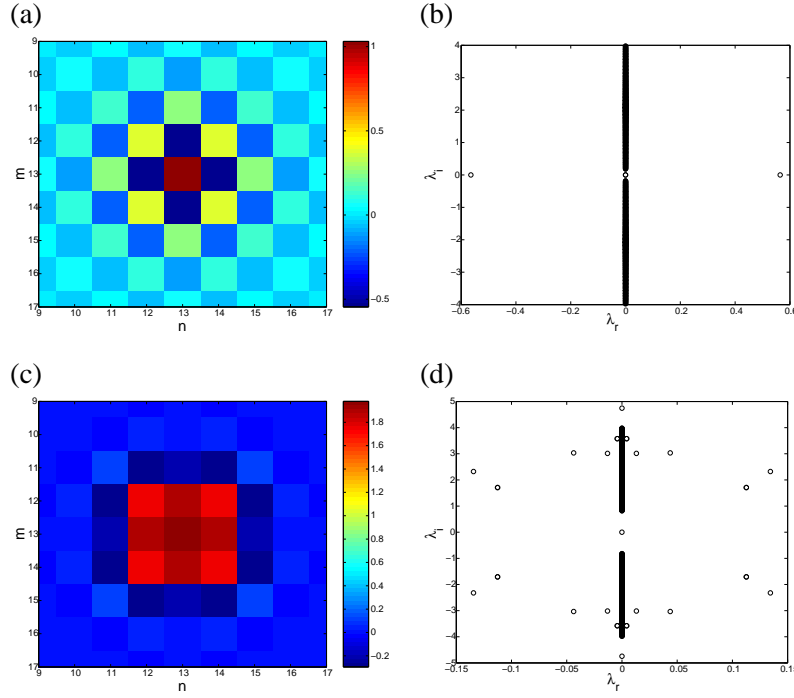

Figure 8: The top panels show the localized gap soliton with $S = 0$, when $C = 0.48$. The bottom panels show a more extended $S = 0$ localized state for $C = 0.4$. Notice that it is highly unstable (this branch becomes unstable for $C > 0.148$).

It is interesting that the stability of the $S = 2$ vortices is also different from what was reported above for the focusing model. While the strongly localized gap-type vortices are unstable for all $C > 0$, as is shown in Fig. 9, and was true in the attractive model, more extended vortex structures with $S = 2$ can be identified as *linearly stable* configurations in the defocusing model (see, e.g., the solutions in the bottom panel of Fig. 9 that are linearly stable for $C < 0.19$). These branches also terminate at $C \approx 0.5$. Higher-order vortices (with $S = 3$ and $S = 4$) have also been found in the defocusing model. However, the latter have been found to be always unstable (in contrast to the vortices in the focusing case), hence we do not discuss them here in detail.

It is straightforward to understand why all the soliton branches in the defocusing case terminate close to $C = 0.5$. Beyond this critical point, the internal frequency of the
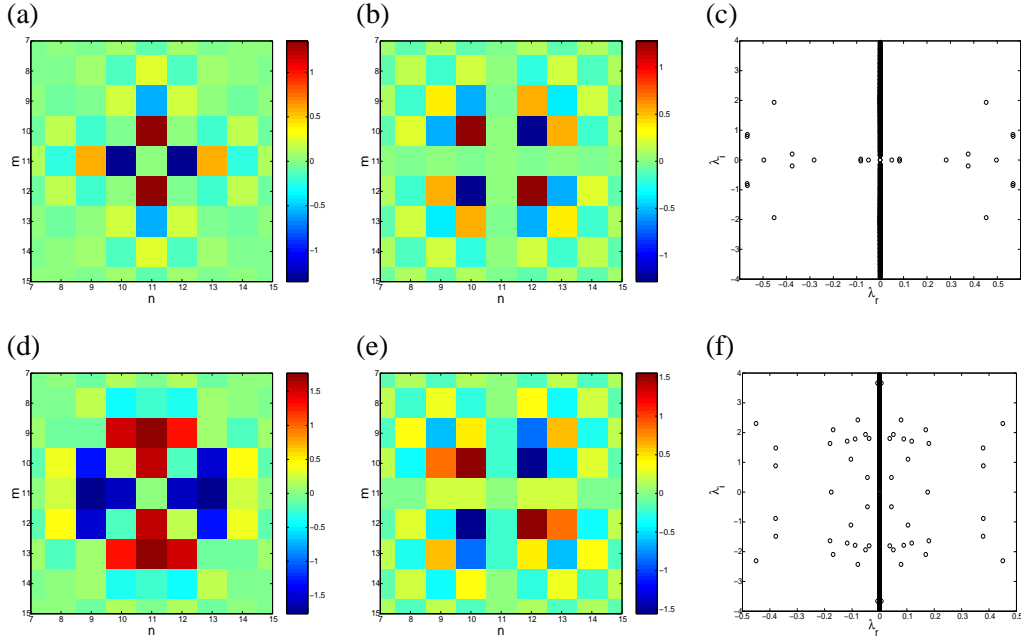
Figure 9: The top panels show the real (left) and imaginary (middle) parts of the unstable $S = 2$ vortex for $C = 0.49$ and $\Lambda = -4$, in the repulsive model. The right panel shows the spectral plane for this case. This vortex is always unstable (similarly to its focusing counterpart). However, the bottom panels indicate a more extended species of the $S = 2$ vortex (it is again shown for $C = 0.49$). The latter one was found to be stable for $C < 0.19$.

discrete soliton ($|\Lambda| = 4$) resonates with the frequencies ω of the linear phonon modes ($\omega = 4C \left[\sin^2(k_n/2) + \sin^2(k_m/2)\right]$, where $k_{m,n}$ are the wavenumbers in the two discrete directions). Hence, solitons cannot exist in the latter case, as a channel for their direct decay into radiation is available.

2.5 Two-Component Vortices

The two-component DNLS model is particularly relevant as a model of BEC droplet arrays composed of a mixture of two different species [49]. The nonlinearly-coupled DNLS equations for the discrete wave functions of the species, $\phi_{m,n}$ and $\psi_{m,n}$, are

$$\left[i\frac{d}{dt} + C\Delta_2 + \begin{pmatrix} |\phi_{m,n}|^2 & \beta|\psi_{m,n}|^2 \\ \beta|\phi_{m,n}|^2 & |\psi_{m,n}|^2 \end{pmatrix}\right]\begin{pmatrix} \phi_{m,n} \\ \psi_{m,n} \end{pmatrix} = 0, \qquad (12)$$

where β is the relative coefficient of the nonlinear interaction between the two species.

In uniform continuum models, two-component (*composite*) solitons, in which one component carries vorticity, are known [48]. We have examined the discrete model (12) for coupled stationary vortex solutions with the set of vorticities $(S_1, S_2) = (1, 1)$ and

$(S_1, S_2) = (1, -1), (3, 3)$ and $(3, -3)$, etc., looking for them in the form

$$\left(\begin{array}{c} \phi_{m,n} \\ \psi_{m,n} \end{array} \right) = e^{i\Lambda t} \left(\begin{array}{c} u_{m,n} \\ v_{m,n} \end{array} \right).$$

The stationary fields in the compound vortices of the types $(+S, +S)$ and $(+S, -S)$ are related in an obvious way,

$$\begin{array}{rcl} (u_{m,n})_{+S,+S} & = & (u_{m,n})_{+S,-S} \\ (v_{m,n})_{+S,+S} & = & \left(v^*_{m,n}\right)_{+S,-S}, \end{array} \tag{13}$$

while their stability may be different. Unlike these symmetric solutions, we were unable to find solutions like $(S_1, S_2) = (3, \pm 1)$.

The region of the dynamical stability of the solutions of the type $(+S, +S)$ was found to be identical to that of the single-component vortex with the topological charge S (obviously, the stability of the latter solution is a necessary condition for the stability of the compound vortex, and our results show that this condition is sufficient as well). For instance, the solutions of the $(1, 1)$ type are stable at $C < 1.6$, cf. Eq. (6).

A striking property of the compound vortices is that the solutions of the $(+S, -S)$ type have a stability region which is, typically, *wider* than that for the $(+S, +S)$ solution. For instance, the $(1, -1)$ vortex was found to be stable at $C < 1.99$, cf. the above-mentioned stability region $C < 1.6$ for its $(1, 1)$ counterpart. The solutions of the $(1, \pm 1)$ types and their stability eigenvalues are displayed together, for $C = 1.6$ [when the solution $(1, 1)$ is unstable and the one $(1, -1)$ is stable], in Fig. 10. These results are obtained for $\beta = 2/3$.

3   Three-Dimensional Vortices

3.1   The Model

The DNLS equation on the 3D cubic lattice with a coupling constant C is [7] [cf. Eq. (1)]

$$i\frac{d}{dt}\phi_{l,m,n} + C\Delta_2\phi_{l,m,n} + |\phi_{l,m,n}|^2 \phi_{l,m,n} = 0, \tag{14}$$

with $\Delta_2\phi_{l,m,n} \equiv \phi_{l+1,m,n} + \phi_{l,m+1,n} + \phi_{l,m,n+1} + \phi_{l-1,m,n} + \phi_{l,m-1,n-1} + \phi_{l,m,n-1} - 6\phi_{l,m,n}$. We seek for localized solutions [sometimes also called intrinsic localized modes (ILMs)] in the same form as in the 2D case, as $\phi_{l,m,n} = \exp(i\Lambda t)u_{l,m,n}$, where stationary functions $u_{l,m,n}$ obey a 3D version of Eq. (2),

$$\Lambda u_{l,m,n} = C\Delta_2 u_{l,m,n} + |u_{l,m,n}|^2 u_{l,m,n}. \tag{15}$$

Solutions to Eq. (15) (generally, complex ones) are obtained by means of the Newton method, with Dirichlet boundary conditions. A 2D counterpart of the expression (3) was used to test the stability of the stationary solutions, which leads to Eqs. (4) and (5), with a difference that, this time, $F_k \equiv -C(u_{k+1} + u_{k-1} + u_{k+N} + u_{k-N} + u_{k+N^2} + u_{k-N^2} - 6u_k) + \Lambda u_k - |u_k|^2 u_k$, and the string index is defined so that $(l, m, n) \mapsto k \equiv l + (m-1)N + (n-1)N^2$.
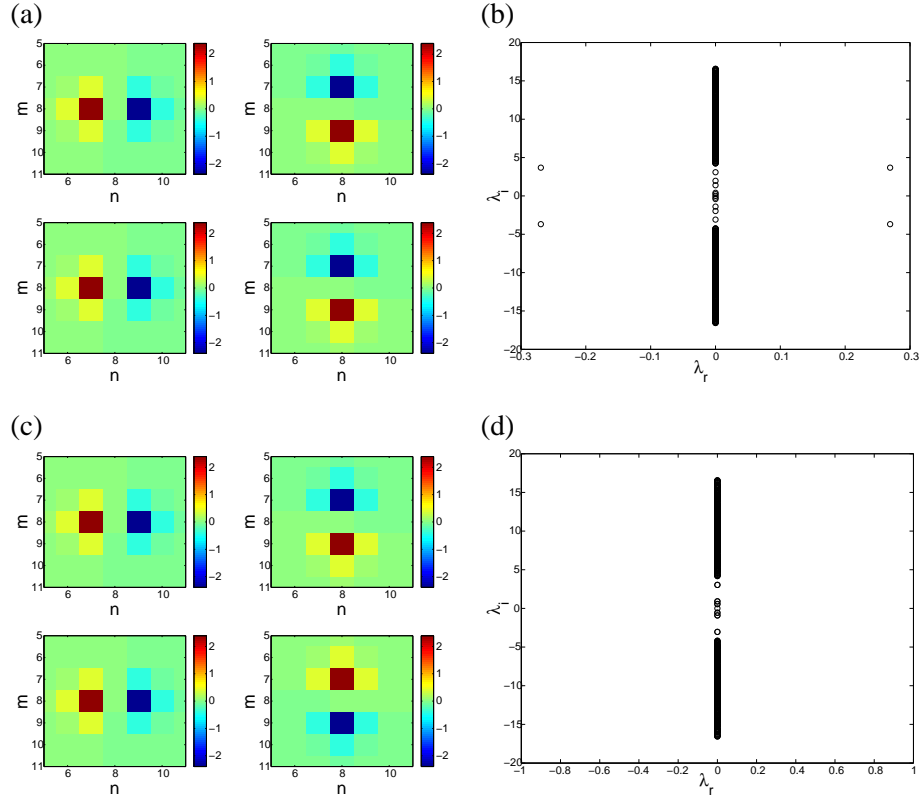
Figure 10: The panels (a) show the real (left) and imaginary (right) parts of the compound vortex with $(S_1, S_2) = (1, 1)$ for $C = 1.6$, and the panel (b) displays the corresponding spectral plane (λ_r, λ_i). The bottom panels show the same features (notice the difference in the spectral plane) for the $(S_1, S_2) = (1, -1)$ solution.

We examine solutions of Eq. (15) by fixing the frequency, $\Lambda = 2$, and varying the coupling C, with the objective to construct ILMs carrying the vorticity S (from 0 to 3). The solutions were generated by a Newton scheme with an initial ansatz motivated by a typical model expression for the 3D vortex soliton in the continuum limit [51],

$$
\begin{aligned}
u_{l,m,n}^{(\mathrm{init})} &= A[(l - l_0) + i(m - m_0)]^S \exp\left(-|n - n_0|\right) \\
&\quad \times \mathrm{sech}\left(\eta\sqrt{(l - l_0)^2 + (m - m_0)^2}\right),
\end{aligned}
\tag{16}
$$

where (l_0, m_0, n_0) is the location of the vortex' center, the lattice angular momentum (which is not a dynamical invariant) is aligned with the axis n, and η is a scale parameter. The Newton algorithm was then iterated until it converged to 1 part in 10^7. Our results are typically shown for $9 \times 9 \times 9$ and $11 \times 11 \times 11$ lattices, but larger ones were also used, without notable differences in the results reported here.

3.2   Results

Basic results for the solutions with different topological charges can be summarized as follows. Ordinary ILMs with $S = 0$ are stable below a critical value $C_{\mathrm{cr}}^{(0)}$ of the coupling constant, which complies with the fact that they are strongly unstable (against the 3D collapse) in the continuum limit of $C \to \infty$ (in fact, $C_{\mathrm{cr}}^{(0)}$ is quite large, and it depends on the size of the numerical lattice). An example of a stable ordinary soliton is shown in Fig. 11. As ILMs with $S = 0$ have the largest stability region, $C < C_{\mathrm{cr}}^{(0)}$, in comparison to topologically charged ones (see below), in the case when they are unstable, they can only be destroyed (decay into phonon waves), rather than transform themselves into ILMs of other types.

(a) $\mathrm{Re}(u_{l,m,n}) = +0.5$ (b) $\mathrm{Re}(u_{l,m,n=5,6})$
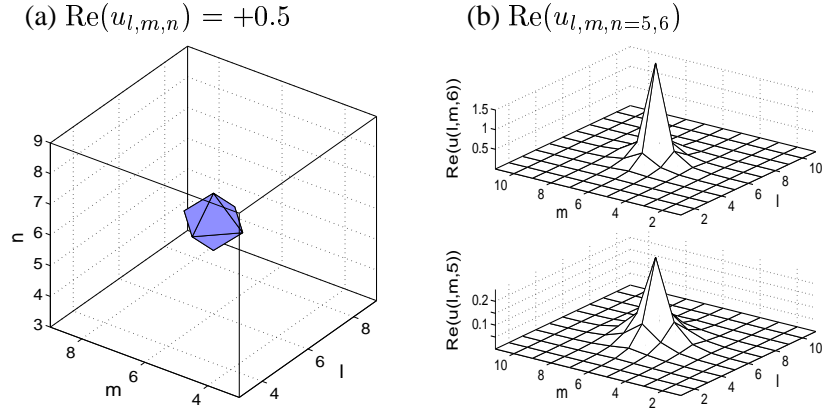

Figure 11: The ILM (intrinsic localized mode) with $S = 0$ in the 3D model is shown for $C = 1$. The left panel shows the shape of the ILM in terms of contours drawn through the lattice sites where $\mathrm{Re}\, u_{l,m,n} = 0.5$. The right panels show 2D cross sections of the solution through the planes $n = 6$ (top) and $n = 5$ (bottom) for the $11 \times 11 \times 11$ DNLS lattice.

3D vortices with $S = 1$ are stable (see Fig. 12) for $C < C_{\mathrm{cr}}^{(1)} = 0.65$, cf. the stability region (6) for the 2D vortex lattice solitons. At the instability threshold, a quartet of complex eigenvalues emerges from collision of two imaginary eigenvalue pairs (for details, see, e.g., Refs. [27, 52]). Numerically simulated development of the instability is displayed in Fig. 12, for a typical case with $C = 0.7 > C_{\mathrm{cr}}^{(1)}$. The instability removes the vortex structure and, as a result, an ordinary ($S = 0$) ILM emerges; obviously, the change of the topological charge is possible in the 3D lattice, as well as in its 2D counterpart, see above.

An example of a 3D vortex ILM with $S = 2$ is shown in Fig. 13 for $C = 0.01$. Similar to its 2D counterpart (see above), this complex solution is unstable through a real eigenvalue pair at all values of C. On the other hand, purely real *stable* solutions, that may be regarded as counterparts of the *quasi-vortices* of the 2D quadrupole-type solutions displayed above, can be found in the 3D case as well; see Fig. 14 for a relevant example. What is more interesting, however, is that the unstable ILMs with $S = 2$ may reshape themselves not downwards, into ones with $S = 0$ or $S = 1$, but rather *upwards*, into a stable vortex ILM with $S = 3$, as seen in Fig. 13.
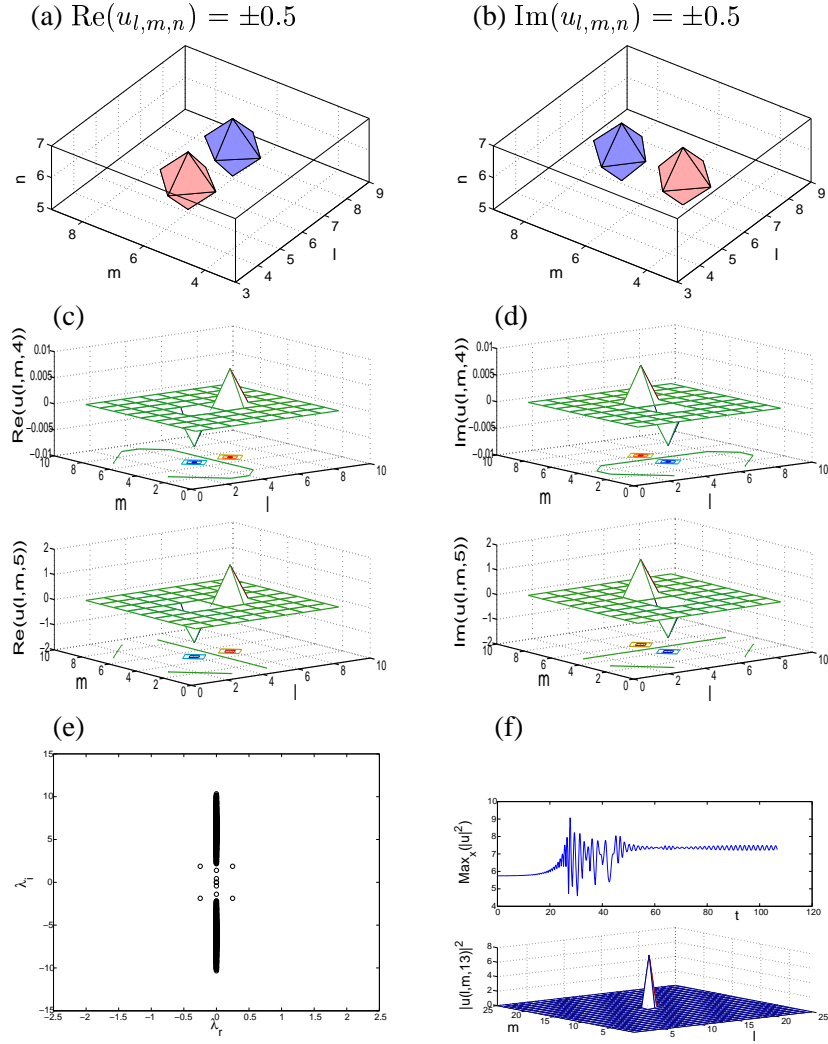
Figure 12: The top panels show level contours at $\mathrm{Re}\, u_{l,m,n} = \pm 0.5$ (left) and $\mathrm{Im}\, u_{l,m,n} = \pm 0.5$ (right) for the three-dimensional vortex ILM with $S = 1$. Red/light-gray and blue/dark-gray surfaces (in the color/black-and-white version) pertain to the levels with $+0.5$ and -0.5 values, respectively. Cross sections of the vortex are shown in four middle panels, (c) and (d). The bottom row displays the development of instability of the vortex for $C = 0.7$, through the time evolution of its amplitude, and a 2D cross section at $t = 100$ [panel (f), top and bottom, respectively]. The unstable vortex transforms itself into an ordinary ILM with $S = 0$. The panel (e) shows the spectral plane (λ_r, λ_i) of the linear-stability eigenvalues for the same unstable vortex.

The stabilization of the vortex ILM with $S = 2$ through spontaneous *increase* of S is a really striking result (feasible only in discrete systems). In Fig. 15, we show the stable $S = 3$ discrete vortex for the same case, $C = 0.01$. The instability of the vortex with $S = 2$ vs. the stability of the vortex with $S = 3$ may be understood, in loose terms (as well as in the

(a) $\mathrm{Re}(u_{l,m,n}) = \pm 0.25$ (b) $\mathrm{Im}(u_{l,m,n}) = \pm 0.25$
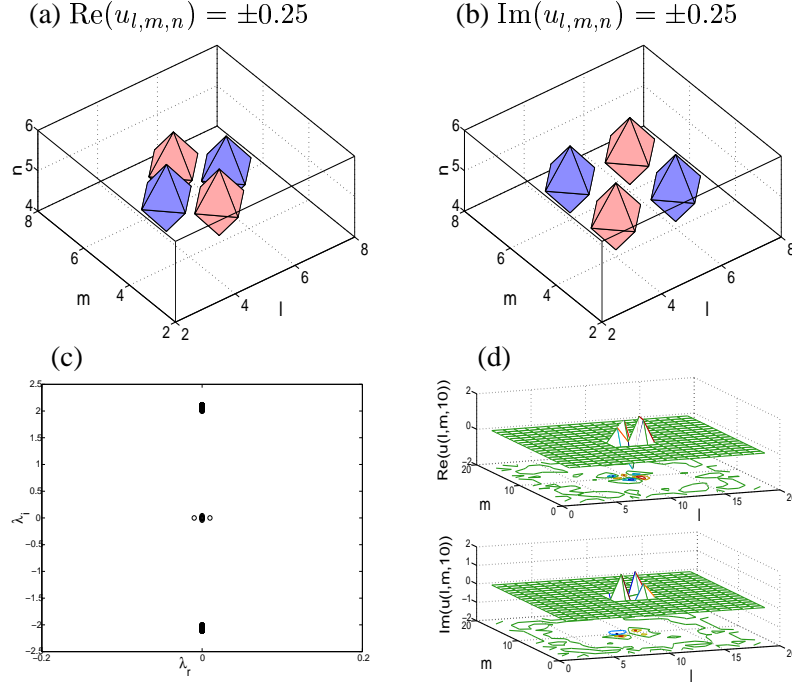
(c)   (d)

Figure 13: The ILM vortex in the 3D lattice, with $S = 2$ for $C = 0.01$. Top panels have the same meaning as in Fig. 4. The panel (c) displays the linear stability eigenvalues, while (d) shows the result of long evolution of this unstable vortex. The eventual state, shown through its 2D cross-sections at $t = 1000$, is a vortex with $S = 3$, which is *stable* for this value of C.

2D case), if one invokes the concept of the lattice-induced *Peierls-Nabarro* (PN) potential acting on the soliton (strictly speaking, in the quasi-continuum approximation). Indeed, it is the PN potential which may stabilize a soliton which would be strongly unstable in the free space. It is seen from Figs. 13 and 15 that the PN potential induced by the cubic lattice is, obviously, a much stronger factor for the soliton with $S = 3$ than with $S = 2$, due to the symmetry difference between the former one and the square lattice (i.e., lines forming the "skeleton" of the $S = 3$ vortex form angles of 120 degrees, as opposed to the right angles of the underlying cubic lattice).

Another striking feature, which is truly unique to the 3D case, is a possibility of the existence of vortex complexes in a multi-component system, with the vortices in different (up to three) components *orthogonal* to each other. We consider, in particular, two coupled 3D DNLS equations, cf. Eqs. (12):

$$\left[i\frac{d}{dt} + C\Delta_2 + \begin{pmatrix} |\phi|^2 & \beta|\psi|^2 \\ \beta|\phi|^2 & |\psi|^2 \end{pmatrix} \right] \begin{pmatrix} \phi \\ \psi \end{pmatrix} = 0, \tag{17}$$

where $(\phi, \psi) = (\phi_{l,m,n}, \psi_{l,m,n})$. As for the 2D case, Eq. 17 describes an array of BEC droplets, composed of a mixture of two different species and trapped in the OL [49]. In the

(a) $\mathrm{Re}(u_{l,m,n}) = \pm0.5$ (b) $\mathrm{Re}(u_{l,m,n=5,6})$
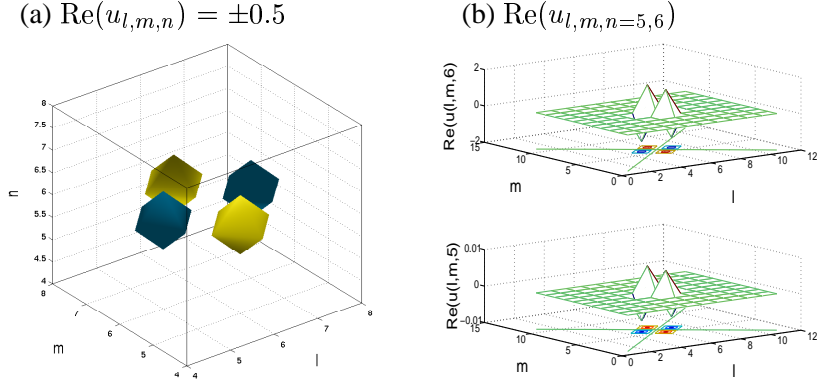

Figure 14: Same as Fig. 11 but for the quasi-vortex with $S = 2$ and for $C = 0.01$. The left panel shows the shape of the quasi-vortex in terms of contours drawn through the lattice sites where $\mathrm{Re}\, u_{l,m,n} = \pm0.5$. The right panels show 2D cross sections of the solution through the planes $n = 6$ (top) and $n = 5$ (bottom) for the $11 \times 11 \times 11$ DNLS lattice.

(a) $\mathrm{Re}(u_{l,m,n}) = \pm0.25$ (b) $\mathrm{Im}(u_{l,m,n}) = \pm0.25$
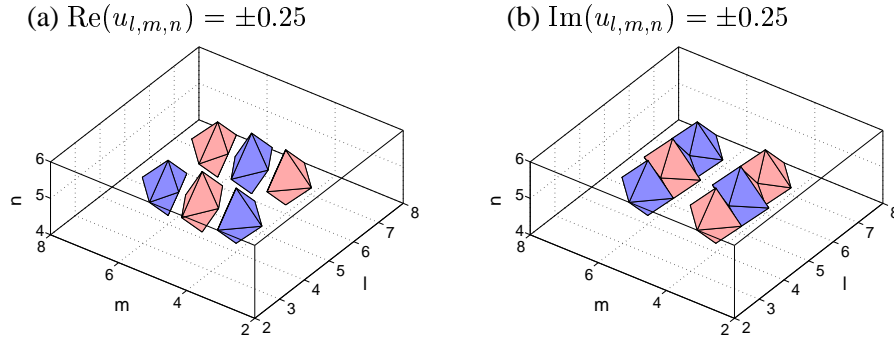

Figure 15: A stable stationary vortex ILM in the 3D lattice with $S = 3$ for $C = 0.01$. The panels have same meaning as top panels in Fig. 4.

case of the above-mentioned model of the photon or polariton field trapped in the lattice of microresonators, ϕ and ψ refer to two different polarizations or distinct cavity modes.

We examine a complex of two orthogonal vortices, in which the one in the first component is directed perpendicular to the (l, m) plane, while, in the second component, the vortex is orthogonal to the (l, n) plane. An example of such a *stable* complex is shown, for $\beta = 0.5$, in Fig. 16. We have found that the orthogonal complexes are stable for $\beta < 1$, and unstable for $\beta > 1$, which can be qualitatively understood in terms of the Hamiltonian of the attractive interaction between the two components, each having the characteristic "doughnut" [51] vortex-soliton shape (in the continuum limit). Indeed, one can roughly estimate the interaction energy through the volume V of the overlap between two cylinders of a radius ρ (which represent long inner holes of the doughnuts) intersecting at an angle θ, $V = (20/3)\rho^3 / \sin\theta$ (the divergence at $\theta \to 0$ is limited by the finite length of the holes). As it follows from here, the interaction energy has a maximum at $\theta = \pi/2$, which

corresponds, by itself, to an unstable equilibrium state of two orthogonal vortices. The equilibrium is transformed into a stable one by the pinning to the PN potential, provided that the interaction is not too strong, i.e., β is not too large.

(a) $\mathrm{Re}(\phi_{l,m,n}) = \pm 0.25$ (b) $\mathrm{Im}(\phi_{l,m,n}) = \pm 0.25$

(c) $\mathrm{Re}(\psi_{l,m,n}) = \pm 0.25$ (d) $\mathrm{Im}(\psi_{l,m,n}) = \pm 0.25$
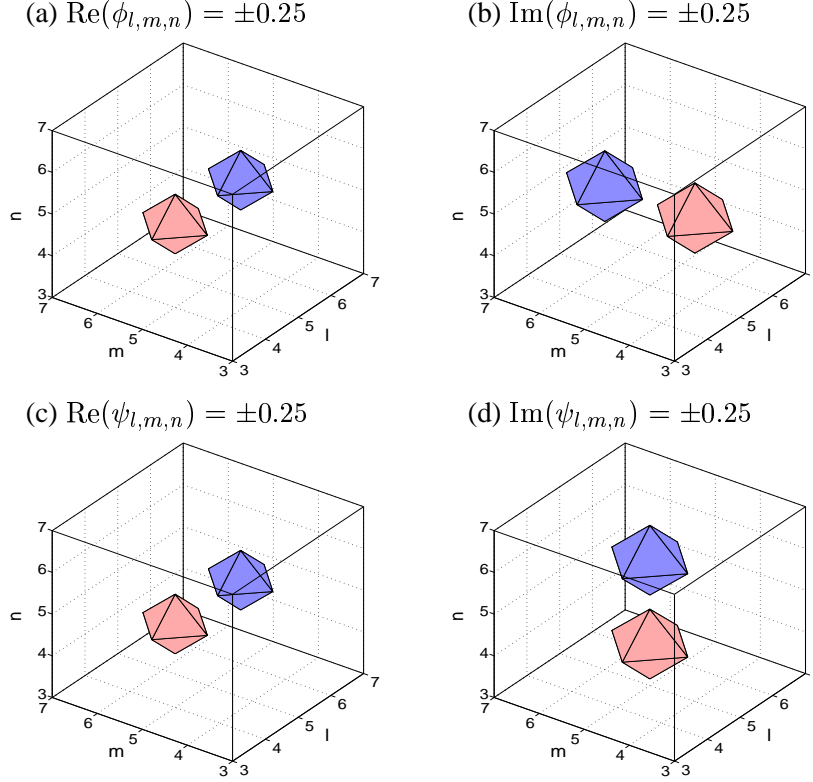
Figure 16: A complex of two orthogonal vortices with $S = 1$ in the two-component 3D system is shown for $C = 0.01$. The top and bottom panels correspond to the two components, and they have the same meaning as the top panels in Fig. 4.

4   Conclusions

In this work, we have constructed and investigated a variety of stable (in appropriate parametric regimes), topologically charged localized vortex states in the two- and three-dimensional versions of the nonlinear dynamical lattice described by the DNLS (discrete nonlinear Schrödinger) equation, as well as a system of two nonlinearly coupled DNLS equations. New objects reported here are stable higher-order vortex solitons (with the vorticity $S > 1$) and quasi-vortices in the 2D model, as well as lattice solitons (ILMs) in its 3D counterpart. Localized vortices in the 2D lattice with the self-defocusing nonlinearity are new entities too.

In the 2D case, the stability region of the true complex vortex with $S = 3$ has been identified. While all the vortices with $S = 2$ are unstable, we have found that they are replaced

by real quasi-vortex solutions of the quadrupole type, which may be stable for sufficiently weak coupling. The stability analysis was based on the calculation of the eigenvalues for small perturbations, and verified against direct simulations. Generally, this interval shrinks with the increase of S. Direct simulations have demonstrated that the unstable $S = 3$ vortices split into a set of two stable solitons with $S = 1$ and $S = 0$, while the quasi-vortex (quadrupole), existing in lieu of the $S = 2$ vortex, transforms itself, in the case of instability, into an ordinary zero-vorticity soliton.

In the 2D two-component model, stability regions of the compound vortex solitons of the $(1, \pm 1)$ types were found. A noteworthy result is that, for the vortices of the $(+S, -S)$ type, the stability area is larger than for their counterparts of the $(+S, +S)$ types.

Localized vortices were also found in the repulsive (defocusing) model and their regions of existence and stability were illustrated. These vortices are tantamount to solutions of the staggered type in the attractive model. It was found that, in this case, the solitons with different values of S exist in two forms, strongly and weakly localized ones. The two types have different stability intervals. In most cases, the stability area is larger for the strongly localized states; however, the weakly localized vortices with $S = 2$ may be stable, in the drastic contrast with the complete instability of this type of the vortices in all the other cases (including the strongly localized $S = 2$ vortices in the repulsive model).

We have constructed vorticity-carrying solitons (alias intrinsic localized modes, ILMs) in the 3D DNLS model too. Stability regions were found for the cases of $S = 0, 1$, and 3. All the 3D ILMs with $S = 2$ are unstable, but their instability develops in quite a nontrivial way, rearranging the soliton into its stable counterpart with the larger vorticity, $S = 3$. Furthermore, the 3D dynamical lattice sustains quite unusual but stable states, such as the two-component vortex complex, with the individual vortices in the components orthogonal to each other. Studying more complex configurations in this setting (such as a complex of three mutually orthogonal vortices in a three-component system), as well as examining interactions between ILMs, are challenging problems for future work.

The results reported in this paper are relevant not only to the general theory of dynamical lattices: the 2D model directly applies to bundled arrays of nonlinear optical waveguides and, indirectly (as the on-site nonlinearity is different), to waveguiding structures in the form of photonic lattices in photorefractive media. In these setups, the results suggest a possibility of existence of new types of spatial optical solitons. In particular, the recent experimental demonstration of stable fundamental discrete vortices in the 2D photonic lattices with self-focusing nonlinearity in Ref. [30] suggests that the higher-order discrete vortices may be observed in the same medium. Experiments were recently performed with vortex masks corresponding to $S = 3$ and $S = 4$ [41]. Another direct application of the theoretical results reported in this paper is the prediction of vortex and quasi-vortex solitons in BECs loaded into strong 2D ("egg-carton") and 3D optical lattices, under realistic experimental conditions.

References

[1] S. Aubry, *Physica* **103D**, 201 (1997); S. Flach and C.R. Willis, *Phys. Rep.* **295**, 181 (1998); *Physica* **119D**, (1999), special volume edited by S. Flach and R.S. MacKay; focus issue edited by Yu.S. Kivshar and S. Flach, *Chaos* **13**, 586 (2003).

[2] A.A. Sukhorukov, Yu.S. Kivshar, H.S. Eisenberg, and Y. Silberberg, *IEEE J. Quantum Elect.* **39**, 31 (2003); U. Peschel, R. Morandotti, J.M. Arnold, J.S. Aitchison, H.S. Eisenberg, Y. Silberberg, T. Pertsch, and F. Lederer, *J. Opt. Soc. Am. B* **19**, 2637 (2002).

[3] A. Trombettoni and A. Smerzi, *Phys. Rev. Lett.* **86**, 2353, (2001); F.Kh. Abdullaev, B.B. Baizakov, S.A. Darmanyan, V.V. Konotop, and M. Salerno, *Phys. Rev.* **A64**, 043606 (2001); F.S. Cataliotti, S. Burger, C. Fort, P. Maddaloni, F. Minardi, A. Trombettoni, A. Smerzi, and M. Inguscio, *Science* **293**, 843 (2001); A. Smerzi, A. Trombettoni, P.G. Kevrekidis, and A.R. Bishop, *Phys. Rev. Lett.* **89**, 170402 (2002); M. Greiner, O. Mandel, T. Esslinger, T. W. Hansch, and I. Bloch, *Nature* (London) **415**, 39 (2002); G. Kalosakas, K.Ø. Rasmussen, and A.R. Bishop *Phys. Rev. Lett.* **89**, 030402 (2002).

[4] E.N. Pelinovsky and S.K. Shavratsky, *Physica* **3D**, 410 (1981).

[5] P. Binder, D. Abraimov, A.V. Ustinov, S. Flach, and Y. Zolotaryuk, *Phys. Rev. Lett.* **84**, 745 (2000); E. Trías, J.J. Mazo, and T.P. Orlando, *Phys. Rev. Lett.* **84**, 741 (2000).

[6] M. Peyrard, and A.R. Bishop, *Phys. Rev. Lett.*, **62**, 2755 (1989); T. Dauxois, M. Peyrard and A.R. Bishop, *Phys. Rev. E*, **47**, R44 (1993); T. Dauxois, M. Peyrard and A.R. Bishop, *Phys. Rev. E*, **47**, 684 (1993); M. Peyrard, T. Dauxois, H. Hoyet, and C.R. Willis, *Physica* **68D**, 104 (1993); A. Campa, and A. Giansanti, *Phys. Rev. E*, **58**, 3585 (1998).

[7] P.G. Kevrekidis, K.Ø. Rasmussen and A.R. Bishop, *Int. J. Mod. Phys. B* **15**, 2833 (2001).

[8] D.N. Christodoulides and R.I. Joseph, *Opt. Lett.* **13**, 794 (1988); A. Aceves, C. De Angelis, G.G. Luther, and A.M. Rubenchik, *Opt. Lett.* **19**, 1186 (1994).

[9] H. Eisenberg, Y. Silberberg, R. Morandotti, A.R. Boyd, and J.S. Aitchison, *Phys. Rev. Lett.* **81**, 3383 (1998); R. Morandotti, U. Peschel, J.S. Aitchison, H.S. Eisenberg, and Y. Silberberg, *Phys. Rev. Lett.* **83**, 2726 (1999); H.S. Eisenberg, R. Morandotti, Y. Silberberg, J.M. Arnold, G. Pennelli, and J.S. Aitchison, *J. Opt. Soc. Am. B* **19**, 2938 (2002); J. Meier, J. Hudock, D. Christodoulides, G. Stegeman, Y. Silberberg, R. Morandotti, J.S. Aitchison, *Phys. Rev. Lett.* **91**, 143907 (2003).

[10] D. Cheskis, S. Bar-Ad, R. Morandotti, J.S. Aitchison, H.S. Eisenberg, Y. Silberberg, D. Ross, *Phys. Rev. Lett.* **91**, 223901 (2003).

[11] J.W. Fleischer, T. Carmon, M. Segev, N.K. Efremidis, and D.N. Christodoulides, *Phys. Rev. Lett.* **90**, 023902 (2003); J.W. Fleischer, M. Segev, N.K. Efremidis, and D.N. Christodoulides, *Nature* **422**, 147 (2003).

[12] I.E. Papacharalampous, P.G. Kevrekidis, B.A. Malomed, and D.J. Frantzeskakis, *Phys. Rev. E* **68**, 046604 (2003).

[13] T. Pertsch, U. Peschel, F. Lederer, J. Burghoff, M. Will, S. Nolte, and A. Tunnermann, *Opt. Lett.* **29**, 468 (2004).

[14] G.L. Alfimov, P.G. Kevrekidis, V.V. Konotop, and M. Salerno, *Phys. Rev. E* **66**, 046608 (2002).

[15] M. Greiner, O. Mandel, T. Esslinger, T.W. Hansch and I. Bloch, *Nature* (London) **415**, 39 (2002).

[16] J.E. Heebner and R.W. Boyd, *J. Mod. Opt.* **49**, 2629 (2002); P. Chak, J.E. Sipe, and S. Pereira, *Opt. Lett.* **28**, 1966 (2003).

[17] D.M. Whittaker and J.S. Roberts, *Phys. Rev. B* **62**, R16247 (2000); P.G. Savvidis and P.G. Lagoudakis, *Sem. Sci. Tech.* **18** , S311 (2003).

[18] N.K. Efremidis, S. Sears, D.N. Christodoulides, J.W. Fleischer, and M. Segev, *Phys. Rev. E* **66**, 046602 (2002).

[19] H. Martin, E.D. Eugenieva, Z. Chen, and D.N. Christodoulides, *Phys. Rev. Lett.* **92**, 123902 (2004).

[20] A.A. Sukhorukov, D. Neshev, W. Krolikowski, and Y.S. Kivshar, *Phys. Rev. Lett.* **92**, 093901 (2004).

[21] Z. Chen, H. Martin, E.D. Eugenieva, J. Xu and A. Bezryadina, *Phys. Rev. Lett.* **92**, 143902 (2004).

[22] D. Neshev, E.A. Ostrovskaya, Yu.S. Kivshar, and W. Krolikowski, *Opt. Lett.* **28**, 710 (2003).

[23] S. Darmanyan, A. Kobyakov, and F. Lederer, *Sov. Phys. JETP* **86**, 682 (1998); P.G. Kevrekidis, A.R. Bishop and K.Ø. Rasmussen, *Phys. Rev. E* **63**, 036603 (2001); T. Kapitula, P.G. Kevrekidis, and B.A. Malomed, *Phys. Rev. E* **63**, 036604 (2001).

[24] P.G. Kevrekidis and V.V. Konotop, *Phys. Rev. E* **65**, 066614 (2002); M. Öster *et al.*, *Phys. Rev. E* **67**, 056606 (2003).

[25] A.A. Sukhorukov and Yu.S. Kivshar, *Opt. Lett.* **27**, 2112 (2002).

[26] P.G. Kevrekidis, B.A. Malomed, and Z. Musslimani, *Eur. Phys. J. D* **23**, 421 (2003); A.V. Gorbach and M. Johansson, *Phys. Rev. E* **67**, 066608 (2003).

[27] B.A. Malomed and P.G. Kevrekidis, *Phys. Rev. E* **64**, 026601 (2001).

[28] P.G. Kevrekidis, B.A. Malomed, and A.R. Bishop, *J. Phys. A: Math. Gen.* **34**, 9615 (2001).

[29] T. Cretegny and S. Aubry, *Phys. Rev. B* **55**, R11929 (1997); M. Johansson, S. Aubry, Yu.B. Gaididei, P.L. Christiansen, and K.Ø. Rasmussen, *Physica D* **119**, 115 (1998).

[30] D.N. Neshev, T.J. Alexander, E.A. Ostrovskaya, Yu.S. Kivshar, H. Martin, I. Makasyuk, and Z. Chen, *Phys. Rev. Lett.* **92**, 123903 (2004).

[31] Jason W. Fleischer, Guy Bartal, O. Cohen, O. Manela, M. Segev, Jared Hudock, and D.N. Christodoulides *Phys. Rev. Lett.* **92**, 123904 (2004)

[32] B.B. Baizakov, B.A. Malomed, and M. Salerno, *Europhys. Lett.* **63**, 642 (2003); H. Sakaguchi and B.A. Malomed, *Europhys. Lett.* **7**2, 698 (2005).

[33] J. Yang and Z. Musslimani, *Opt. Lett.* **23**, 2094 (2003).

[34] B.B. Baizakov, B.A. Malomed, and M. Salerno, *Phys. Rev. A* **7**0, 053613 (2004).

[35] E.A. Ostrovskaya and Yu.S. Kivshar, *Phys. Rev. Lett.* **9**3, 160405 (2004).

[36] H. Sakaguchi and B.A. Malomed, *J. Phys. B: At. Mol. Opt. Phys.* **37**, 2225 (2004).

[37] T.J. Alexander, A.A. Sukhorukov, Yu.S. Kivshar, *Phys. Rev. Lett.* **9**3, 063901 (2004).

[38] L.-C. Crasovan, B.A. Malomed, and D. Mihalache, *Pramana Journal of Physics* **57**, 1041 (2001); B.A. Malomed, L.-C. Crasovan, and D. Mihalache, *Physica D* **161**, 187 (2002).

[39] R.L. Pego and H.A. Warchall, *J. Nonlin. Sci.* **12**, 347 (2002).

[40] D. Mihalache, D. Mazilu, B.A. Malomed, and F. Lederer, *Phys. Rev. E* **6**9, 066614 (2004).

[41] J. Yang, I. Makasyuk, P.G. Kevrekidis, H. Martin, B.A. Malomed, D.J. Frantzeskakis, and Z. Chen, *Phys. Rev. Lett.* **9**4, 113902 (2005).

[42] M. Johansson and S. Aubry, *Phys. Rev. E* **61**, 5864 (2000).

[43] J.-C. van der Meer, *Nonlinearity* **3**, 1041 (1990).

[44] D.V. Skryabin *Phys. Rev. E* **64**, 055601 (2001)

[45] T. Kapitula, P.G. Kevrekidis and B. Sandstede, *Physica D* **2**01, 199 (2005).

[46] C. Menotti, A. Smerzi and A. Trombettoni, *New J. Phys.* **5**, 112 (2003).

[47] P.G. Kevrekidis, K.Ø. Rasmussen, and A.R. Bishop *Phys. Rev. E* **61**, 4652 (2000).

[48] Z.H. Musslimani, M. Segev, D.N. Christodoulides, and M. Soljacic, *Phys. Rev. Lett.* **84**, 1164 (2000).

[49] C.J. Myatt, E.A. Burt, R.W. Ghrist, E.A. Cornell, and C.E. Wieman, *Phys. Rev. Lett.* **78**, 586 (1997).

[50] B.B. Baizakov, V.V. Konotop, and M. Salerno, J. Phys. B **35**, 5105 (2002); B.B. Baizakov, B.A. Malomed, and M. Salerno, *Europhys. Lett.* **63**, 642 (2003).

[51] D. Mihalache, D. Mazilu, L.-C. Crasovan, I. Towers, A.V. Buryak, B.A. Malomed, L. Torner, J.P. Torres, and F. Lederer. *Phys. Rev. Lett.* **88**, 073902 (2002); D. Mihalache, D. Mazilu, L.-C. Crasovan, I. Towers, B.A. Malomed, A.V. Buryak, L. Torner, and F. Lederer. *Phys. Rev. E* **66**, 016613 (2002).

[52] P.G. Kevrekidis, B.A. Malomed, Z. Chen, and D.J. Frantzeskakis, *Phys. Rev. E.* **7**0, 056612 (2004).